

A Theory of Topological Kondo Insulators

Maxim Dzero¹, Kai Sun², Piers Coleman^{3,4} and Victor Galitski²

¹ *Department of Physics, Kent State University, Kent, OH 44242, USA*

² *Joint Quantum Institute and Condensed Matter Theory Center,*

Department of Physics, University of Maryland, College Park, MD 20742, USA

³ *Center for Materials Theory, Rutgers University, Piscataway, NJ 08854, USA*

⁴ *Department of Physics, Royal Holloway, University of London, Egham, Surrey TW20 0EX, UK*

(Dated: November 16, 2011)

We examine how the properties of the Kondo insulators change when the symmetry of the underlying crystal field multiplets is taken into account. We employ the Anderson lattice model and consider its low-energy physics. We show that in a large class of crystal field configurations, Kondo insulators can develop a topological non-trivial ground-state. Such topological Kondo insulators are adiabatically connected to non-interacting insulators with unphysically large spin-orbit coupling, and as such may be regarded as interaction-driven topological insulators. We analyze the entanglement entropy of the Anderson lattice model of Kondo insulators by evaluating its entanglement spectrum. Our results for the entanglement spectrum are consistent with the surface state calculations. Lastly, we discuss the construction of the maximally localized Wannier wave functions for generic Kondo insulators.

PACS numbers: 71.27.+a, 75.20.Hr, 74.50.+r

I. INTRODUCTION

Topological insulators are a novel class of materials in which strong spin-orbit interaction leads to the inversion of the band gap (See Ref. 1 and 2 and references therein). In 3D, this inversion results in chiral metallic surface states due to a formation of a single Dirac cone inside the gap³⁻⁷. Among materials which exhibit this behavior, for example, HgTe, Bi₂Se₃, Bi_{1-x}Sb_x, Bi₂Te₃ and TlBiTe₂, the chiral structure of the surface states has been confirmed experimentally⁸⁻¹¹.

The emergence of surface modes in topological insulators is a band structure effect which can be understood without invoking interactions. There is great current interest in the possibility of interaction driven topological phenomena. Up until now there are no experimental examples of interaction-driven topological insulators that preserve time-reversal symmetry. However, several theoretical proposals have been put forward: 2D topological insulators via spontaneous symmetry breaking in bilayer graphene and optical lattice systems¹²⁻¹⁵, topological Mott insulating phase in Ir-based pyrochlore oxides A₂Ir₂O₇ with A=Nd,Pr¹⁶⁻¹⁹, Kondo insulators with the most salient example of SmB₆²⁰ and insulating behavior in filled skutteridites²¹. In this paper we focus on general principles governing the emergence of chiral metallic states in Kondo insulators. Throughout this paper, we use the term “Kondo insulator” in its broadest sense, including both mixed valent materials²² such as SmB₆ and YbB₁₂ and those in the more localized limit, such as Ce₃Bi₄Pt₃.

Kondo insulators are a type of heavy fermion material, first discovered forty years ago²³, in which highly renormalized *f*-electrons hybridize with conduction electrons to form a completely filled band of quasiparticles with excitation gaps in the millivolt range²⁴⁻²⁷. Because Kondo insulators appear as a result of strong interactions, one might think that their excitations and their ground-states are adiabatically connected to trivial non-interacting band insulators²⁸. However, before jumping to this conclusion one needs to be careful, for in the

renormalization process the width of the heavy electron bands drops far below the characteristic size of the spin-orbit interactions, driving the physics to a new fixed point characterized by infinite spin-orbit coupling in the localized bands. Indeed, we shall show that topological Kondo insulators are adiabatically connected to non-interacting topological insulators with an unphysically large value of the spin-orbit coupling, and in this sense, they are interaction-driven insulators.

One of the most important features of the *f*-electron systems in general and Kondo insulators in particular is that the *f*-electron states are classified with respect to their momentum \mathbf{k} , total angular momentum J and its z -axis component M , while conduction electron states are described by a momentum and a spin σ . When an *f*-electron escapes into the conduction sea, it hybridizes with a spin-orbit coupled Wannier state of the conduction electrons that has the same symmetry as the *f*-state. The spin-orbit coupled Wannier states of the conduction electrons are then decomposed in terms of plane-wave states and this gives rise to momentum-dependent form factors with symmetries that are uniquely determined by the local symmetry of the *f*-states. In this way, the form factors encode the effect of the strong spin-orbit coupling. More importantly, these form factors also define the underlying symmetry of the hybridization amplitude and gap which develops below the “Kondo temperature” T_K at which heavy quasi-particles develop. One of the key properties of the spin-orbit coupled *f*-state, is an odd-parity wavefunction. It is the protected odd-parity of the *f*-states that provides the driving force for the formation of topological insulating states.

The dimension of the form factor matrix is determined by the degeneracy of the underlying ground state *f*-ion multiplet. In the crystalline environment the $(2J + 1)$ multiplet degeneracy is lifted by the crystalline fields. For half-integer values of J the lowest possible degenerate multiplet is a Kramers doublet, which means that the form factor is a two-dimensional matrix. For the integer values of J the crystal field can fully lift degeneracy of the multiplet. This situation corresponds to

the non-magnetic state of the f -ion and currently there are no known examples of such Kondo insulators. Thus, in this article we will only focus on the magnetic ions with half-integer values of the total angular momentum.

As mentioned above, the symmetry of the lowest lying multiplet determines the symmetry of the hybridization amplitude. Generically, two possible scenarios can arise depending on whether the hybridization contains nodes or not. For a small, but important subset of these systems, the hybridization contains nodes. In this case, the Kondo insulating state is replaced by a heavy semi-metal with a pseudogap, as in the case of CeNiSn or CeRhSb. If the nodes correspond to touching of the two non-degenerate bands with linear dispersion, the system becomes a Weyl semi-metal, where topologically-protected surface modes emerge²⁹. Note, that the lifting of degeneracy can only happen due to onset of magnetic order. The magnetic moments may appear as a result of incomplete screening similarly to what happens in CeCoIn5, for example.

In our previous work, we demonstrated within a mean-field model, that in the large class of systems without nodes in the hybridization gap, Kondo insulators can develop topological insulating ground-states²⁰. In this paper we develop this idea in detail, providing mathematical details of the construction of the wavefunction and explicitly computing the surface modes for a topological Kondo insulator.

Although attempts to establish the general principle determining the relative position of the crystal field multiplets have been made^{30–32}, but no such principle has yet been discovered. Experimentally, however, the symmetry of the lowest lying as well as excited multiplets can be detected, for example, by inelastic neutron scattering spectroscopy³³. Nevertheless, by assuming a specific symmetry of the ground state multiplet one is able to theoretically predict the physical properties of a Kondo insulator. In addition, it provides multiple ways to verify them experimentally. To be more precise, the presence of the chiral states on the surface of Kondo insulators will allow one to indicate unambiguously the symmetry of the lowest lying multiplet.

Apart from going beyond the brief description of topological Kondo insulators reported in Ref. 20, we will discuss the topological properties of the eigenfunctions of the model Hamiltonian describing the Kondo insulators. We will start with a short review of the model and recently obtained results. We evaluate the entanglement spectrum for simplest model of the Kondo insulator corresponding to the nearest neighbors tight-binding approximation for the conduction bands and a Kramers doublet. We also discuss the choice of the proper basis for construction of the maximally localized Wannier functions for the Kondo insulators. We show that Wannier functions can be constructed on the basis composed of the linear combination between the conduction and f -electron states. Finally, we provide a short review of available experimental data which points towards the existence of the chiral surface states in Kondo insulators.

II. ANDERSON LATTICE MODEL

We begin with writing down the model Hamiltonian to describe the physics of the Kondo insulators. In what follows we will consider the most general case by assuming that there are N_c conduction bands, so that the Hamiltonian describing conduction electrons is

$$H_c = \sum_{l=1}^{N_c} \sum_{\mathbf{k}, \sigma} \xi_{l\mathbf{k}} c_{\mathbf{k}\sigma}^{(l)\dagger} c_{\mathbf{k}\sigma} \quad (1)$$

where $\xi_{l\mathbf{k}}$ is the dispersion of the l th band of conduction electrons, σ is the spin index and $c_{\mathbf{k}\sigma}^{(l)\dagger}$ is a conduction electron creation operator. Consequently, the Hamiltonian which describes the f -electrons is:

$$H_f = \sum_j \sum_{\alpha=1}^{N_\Gamma} \epsilon_{f\Gamma} f_{j\alpha}^\dagger f_{j\alpha} + U \sum_{i\alpha\alpha'} f_{i\alpha}^\dagger f_{i\alpha} f_{i\alpha'}^\dagger f_{i\alpha'}. \quad (2)$$

where $f_{j\alpha}^\dagger$ creates an f -electron on site j in a state α of a lowest lying multiplet N_Γ -degenerate multiplet denoted by Γ (see below), ϵ_f is the f -electron energy and $U > 0$ is the strength of the Hubbard interaction between the f -electrons. We emphasize that index α is not a spin index due to the presence of the strong spin-orbit coupling. Generally states belonging to the multiplet Γ are described by the total angular momentum J and z -component M or some linear superposition of those states and in the second term of Eq. (2), the summation is restricted to $\alpha \neq \alpha'$.

Finally the term describing how electrons in N_c conduction bands are hybridized with localized f -electrons is

$$H_h = \sum_{l=1}^{N_c} \sum_{j,\alpha=1}^{N_\Gamma} \left[V_{i\sigma,j\alpha}^{(l)} c_{i\sigma}^{(l)\dagger} f_{j\alpha} + \text{h.c.} \right], \quad (3)$$

Here $V_{i\sigma,j\alpha}^{(l)}$ is a non-local hybridization matrix element between the conduction electrons in l th band and localized f -electrons. Thus, the periodic Anderson model Hamiltonian, which is the basis for our subsequent discussion, reads:

$$H_{PAM} = H_c + H_f + H_h \quad (4)$$

The hybridization matrix elements $V_{i\sigma,j\alpha}^{(l)}$ can be written as follows :

$$V_{i\sigma,j\alpha}^{(l)} = V_l \sum_{\mathbf{k}\sigma} [\Phi_{\Gamma\mathbf{k}}]_{\alpha\sigma} e^{i\mathbf{k}\cdot(\mathbf{R}_i - \mathbf{R}_j)}, \quad (5)$$

where V_l is the hybridization amplitude and the form factors $[\Phi_{\Gamma\mathbf{k}}]_{\alpha\sigma}$ are $(2J + 1) \times 2$ dimensional matrices given by:

$$[\Phi_{\Gamma\mathbf{k}}]_{\alpha\sigma} = \langle k\Gamma\alpha | \mathbf{k}\sigma \rangle \quad (6)$$

Since in this paper we will be discussing the materials when an f -ion is in the valence state with $J = 5/2$ (f^1 for cerium or f^3 for samarium) it follows

$$[\Phi_{\Gamma\mathbf{k}}]_{\alpha\sigma} = \sum_{m \in \{-3,3\}} \left\langle \Gamma\alpha \left| 3m, \frac{1}{2}\sigma \right\rangle \tilde{Y}_{m-\sigma}^3(\mathbf{k}) \quad (7)$$

and

$$\tilde{Y}_M^3(\mathbf{k}) = \frac{1}{Z} \sum_{\mathbf{R} \neq 0} Y_M^3(\hat{\mathbf{R}}) e^{i\mathbf{k} \cdot \mathbf{R}} \quad (8)$$

is a tight-binding generalization of the spherical Harmonics that preserves the translational symmetry of the hybridization, $\Phi(\mathbf{k}) = \Phi(\mathbf{k} + \mathbf{G})$, where \mathbf{G} is reciprocal lattice vector. Here, \mathbf{R} are the positions of the Z nearest neighbor sites around the magnetic ion. Note, that deriving (6) we have assumed that the symmetry of the conduction electron amplitude coincides with the symmetry of the f -ion multiplet^{34,35}. Consequently, we treat the system with only one hybridization channel. Now let us recall the definition of the form factors:

$$[\Phi_{\hat{\mathbf{k}}}]_{\alpha\sigma} = \sum_{M=-5/2}^{5/2} \langle k\alpha | JM \rangle \langle JM | \hat{\mathbf{k}}\sigma \rangle, \quad (9)$$

where $\langle JM | \hat{\mathbf{k}}\sigma \rangle$ is a $(2J+1) \times 2$ matrix whose elements are given by $\sigma \sqrt{\frac{5-M\sigma}{7}} Y_{M-\frac{1}{2}\sigma}^3(\hat{\mathbf{k}})$. The elements of the matrix $\langle k\alpha | JM \rangle$ are determined by the specific choice of the f -ion multiplet and the corresponding wave-functions denoted by $|\Gamma\alpha\rangle$. As we have already mentioned above, we will focus our discussion on the case of f -ion with $J = 5/2$. This situation is relevant for all known f -electron Kondo insulators. Consequently, in a cubic crystal field environment, the magnetic ion multiplet is split into a doublet

$$|\Gamma_1^{(c)} \pm\rangle = \pm \sqrt{\frac{5}{6}} \left| \pm \frac{3}{2} \right\rangle \mp \sqrt{\frac{1}{6}} \left| \mp \frac{5}{2} \right\rangle \quad (10)$$

and a quartet

$$\begin{aligned} |\Gamma_2^{(c)} \pm\rangle &= \pm \sqrt{\frac{1}{6}} \left| \mp \frac{3}{2} \right\rangle \pm \sqrt{\frac{5}{6}} \left| \pm \frac{5}{2} \right\rangle, \\ |\Gamma_3^{(c)} \pm\rangle &= \pm \left| \pm \frac{1}{2} \right\rangle, \end{aligned} \quad (11)$$

so that for this case the matrix $\langle k\alpha | JM \rangle$ is

$$\begin{aligned} \langle k\alpha_i | JM \rangle &= \\ &= \begin{pmatrix} 0 & -\sqrt{\frac{1}{6}} & 0 & 0 & 0 & -\sqrt{\frac{5}{6}} \\ 0 & 0 & 1 & 0 & 0 & 0 \\ 0 & 0 & 0 & -1 & 0 & 0 \\ \sqrt{\frac{5}{6}} & 0 & 0 & 0 & \sqrt{\frac{1}{6}} & 0 \\ 0 & \sqrt{\frac{5}{6}} & 0 & 0 & 0 & -\sqrt{\frac{1}{6}} \\ \sqrt{\frac{1}{6}} & 0 & 0 & 0 & -\sqrt{\frac{5}{6}} & 0 \end{pmatrix} \end{aligned} \quad (12)$$

In a tetragonal crystal field environment, relevant for Ce-based Kondo insulators, the Ce multiplet is split into three doublets:

$$\begin{aligned} |\Gamma_1^{(t)} \pm\rangle &= |\pm 1/2\rangle, \\ |\Gamma_2^{(t)} \pm\rangle &= \cos(\beta) |\mp 3/2\rangle + \sin(\beta) |\pm 5/2\rangle, \\ |\Gamma_3^{(t)} \pm\rangle &= \sin(\beta) |\mp 3/2\rangle - \cos(\beta) |\pm 5/2\rangle, \end{aligned} \quad (14)$$

where the mixing angle β defines orientation of the corresponding states. In an orthorhombic environment, the Kramer's doublets are generally described by a linear superposition of all three wave-functions^{30,32}

$$|\Gamma^{(ortho)} \pm\rangle = u |\pm 1/2\rangle + v |\mp 3/2\rangle + w |\pm 5/2\rangle. \quad (15)$$

Having provided the scheme for the computation of the form-factors we proceed with the discussion of the low-energy properties of our model (4) of Kondo insulators.

III. LOW-ENERGY THEORY FOR Ce-BASED KONDO INSULATORS

The low-energy properties of the model (4) are described in terms of renormalized quasiparticles formed via strong hybridization between the c - and f - states and on-site repulsion U between the f -electrons. In the regime where the f states are predominantly localized, $U \sim W$ (W is the bandwidth), we can neglect the momentum dependence of the f -electron self-energy $\Sigma_f(\mathbf{k}, \omega) \simeq \Sigma_f(\omega)$.

Below we discuss the topological properties of the effective low-energy model. To make our discussion more tractable, we will consider separately several experimentally relevant cases. In what follows we discuss the simplest case of the single conduction band and Kramers doublet as a ground state multiplet of the magnetic ion. This is done with an eye toward the transport experiments on the Ce-based Kondo insulators^{36,37}.

A. single conduction band hybridized with the Kramers doublet: Ce-based Kondo insulators

In order to derive an effective low-energy model for Kondo insulators, we first introduce the following correlation functions for c - and f -electrons:

$$\begin{aligned} G_{cc}(\mathbf{k}, \tau) &= -\langle \hat{T}_\tau \{ c_{\mathbf{k}\sigma}(\tau) c_{\mathbf{k}\sigma}^\dagger(0) \} \rangle, \\ G_{ff}(\mathbf{k}, \tau) &= -\langle \hat{T}_\tau \{ f_{\mathbf{k}\alpha}(\tau) f_{\mathbf{k}\alpha}^\dagger(0) \} \rangle, \end{aligned} \quad (16)$$

By writing down equations of motion for the c -operators with the Hamiltonian (4) and going into Matsubara frequency representation we derive the following relation:

$$G_{cc}(\mathbf{k}, i\omega) = G_{cc}^{(0)}(\mathbf{k}, i\omega) + \frac{|V|^2 \Delta_{\mathbf{k}}^2}{(i\omega - \xi_{\mathbf{k}})^2} G_{ff}(\mathbf{k}, i\omega) \quad (17)$$

with $\Delta_{\mathbf{k}}^2 = \frac{1}{2} \text{Tr}[\Phi_{\Gamma_{\mathbf{k}}}^\dagger \Phi_{\Gamma_{\mathbf{k}}}]$ and $G_{cc}^{(0)}(\mathbf{k}, i\omega)$ is a conduction electron propagator in the absence of interactions. If we denote the f -electron self-energy by $\Sigma_f(\mathbf{k}, \omega)$ and keep in mind that this self-energy appears as a result of Hubbard correlations only, then it follows:

$$G_{ff}(\mathbf{k}, i\omega) = \left[i\omega - \epsilon_f - \Sigma_f(\mathbf{k}, i\omega) - \frac{|V|^2 \Delta_{\mathbf{k}}^2}{i\omega - \xi_{\mathbf{k}}} \right]^{-1} \quad (18)$$

Next we assume that the self-energy is very weakly dependent on momentum, $\Sigma_f(\mathbf{k}, i\omega) \simeq \Sigma_f(k_F, i\omega)$ (k_F is the conduction electron's Fermi momentum) and expand it to the lowest

order in Matsubara frequency:

$$\Sigma_f(\mathbf{k}, i\omega) \simeq \Sigma_f(k_F, i\omega) + i\omega \left[\frac{\partial \Sigma_f(k_F, i\omega)}{\partial(i\omega)} \right]_{i\omega \rightarrow 0} \quad (19)$$

Taking into account expressions (18,19), for the correlators we find

$$G_{cc}(\mathbf{k}, i\omega) = \frac{i\omega - \varepsilon_f}{(i\omega - \xi_{\mathbf{k}})(i\omega - \varepsilon_f) - |\tilde{V}|^2 \Delta_{\mathbf{k}}^2}, \quad (20)$$

$$G_{ff}(\mathbf{k}, i\omega) = \frac{i\omega - \xi_{\mathbf{k}}}{(i\omega - \xi_{\mathbf{k}})(i\omega - \varepsilon_f) - |\tilde{V}|^2 \Delta_{\mathbf{k}}^2},$$

where $\xi_{\mathbf{k}} = -2t \sum_{a=x,y,z} \cos k_a$ is the bare spectrum of conduction electrons taken relative to the chemical potential, $\varepsilon_f = Z[\varepsilon_f + \Sigma_f(0)]$ is the renormalized f -level, $\tilde{V} = \sqrt{Z}V$ and $Z = (1 - \partial \Sigma_f(k_F, \omega)/\partial \omega)_{\omega=0}^{-1}$. These propagators correspond to the following effective Hamiltonian³¹:

$$\mathcal{H}_{eff}(\mathbf{k}) = \begin{pmatrix} \xi_{\mathbf{k}} \underline{1} & \tilde{V} \Phi_{\Gamma \mathbf{k}}^\dagger \\ \tilde{V} \Phi_{\Gamma \mathbf{k}} & \varepsilon_f \underline{1} \end{pmatrix}, \quad (21)$$

Here $\underline{1}$ denotes the unit 2×2 matrix. The KI is formed if the chemical potential of the quasiparticles lies inside the hybridization gap, separating the two bands with the spectra

$$E_{\pm}(\mathbf{k}) = \frac{1}{2} [\xi_{\mathbf{k}} + \varepsilon_f \pm \sqrt{(\xi_{\mathbf{k}} - \varepsilon_f)^2 + 4 |\tilde{V} \Delta_{\mathbf{k}}|^2}].$$

To discuss the topological properties of our effective model for the KI (21), we need to consider separately the form factors for different Γ 's. It is convenient to distinguish these states according to their orbital symmetry parameterized by the index $a = 1, 2, 3$ and the pseudo-spin quantum number ($\alpha = \pm$)³². Hence, we have $f_{1\pm}^\dagger |0\rangle = |\pm 1/2\rangle$, $f_{2\pm}^\dagger |0\rangle = |\pm 3/2\rangle$, and $f_{3\pm}^\dagger |0\rangle = |\pm 5/2\rangle$.

The momentum-dependence of the hybridization gap $\Delta_a(\mathbf{k})$ follows from Eq. (7). At small momenta \mathbf{k} , $\Delta_1(\mathbf{k}) = \frac{1}{12} \sqrt{\frac{3}{\pi}} [12 \cos(2\theta) + 5(3 + \cos(4\theta))]^{1/2}$, $\Delta_2(\mathbf{k}) = \frac{1}{8} \sqrt{\frac{3}{\pi}} |\sin \theta| [17 + 15 \cos(2\theta)]^{1/2}$, and $\Delta_3(\mathbf{k}) = \frac{1}{4} \sqrt{\frac{15}{2\pi}} \sin^2 \theta$, where θ and ϕ define the direction of the unit vector $\hat{\mathbf{k}}$, associated with the point on the Fermi surface. Note that the hybridization gap has a line of nodes along the z -axis for the shapes $a = 2, 3$, but generic combinations of all three form-factors characteristic of contain no nodes. The key results of this Section are most simply illustrated using the nodeless $a = 1$ Kramers doublet as the ground-state of the magnetic ion.

To analyze the topology of the bands we use the fact that topology is invariant under any adiabatic deformation of the Hamiltonian. We begin our study with a tight-binding model for a KI on a simple cubic lattice. Our choice of hybridization ensures that the mean-field Hamiltonian (Eq. 21) is a periodic function satisfying $\mathcal{H}_{eff}(\mathbf{k}) = \mathcal{H}_{eff}(\mathbf{k} + \mathbf{G})$. The technical analysis is readily generalized to more complicated cases as discussed below. The most important element of the analysis is the odd parity form factor of the f electrons, $\Phi_a(\mathbf{k}) = -\Phi_a(-\mathbf{k})$. This parity property is the only essential input as far as the topological structure is concerned.

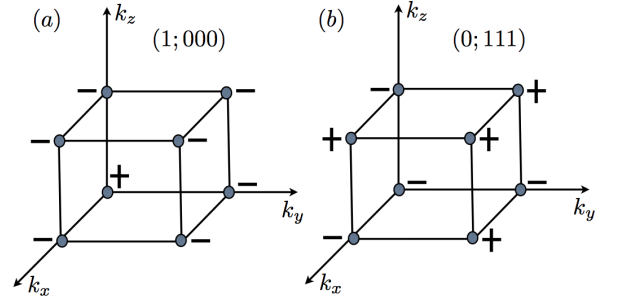


FIG. 1: Two topological classes can be realized in our model of Kondo insulators for $\varepsilon_f < 2t$ (see text). The first class with index $\nu = (1;000)$ corresponds to a strong topological insulator and is realized when $\varepsilon_f < -2t$. The second class with index $\nu = (0;111)$ is realized for $-2t < \varepsilon < 2t$. When the renormalized position of the f -level is at the boundaries, $\varepsilon_f = \pm 2t, \pm 6t$ the system is metallic.

B. calculation of topological indices

In Ref. 38, Fu and Kane demonstrate that in an insulator with time-reversal and space-inversion symmetry, the topological structure is determined by parity properties at the eight high-symmetry points, \mathbf{k}_m^* , in the 3D BZ which are invariant under time-reversal, up to a reciprocal lattice vector: $\mathbf{k}_m^* = -\mathbf{k}_m^* + \mathbf{G}$. In our case, these symmetries require that $\mathcal{H}_{eff}(\mathbf{k}) = P \mathcal{H}_{eff}(-\mathbf{k}) P^{-1}$ and $\mathcal{H}_{eff}(\mathbf{k})^T = \mathcal{T} \mathcal{H}_{eff}(-\mathbf{k}) \mathcal{T}^{-1}$, where the parity matrix P and the unitary part of the time-reversal operator \mathcal{T} are given by

$$P = \begin{pmatrix} \underline{1} & \\ & -\underline{1} \end{pmatrix}, \quad \mathcal{T} = \begin{pmatrix} i\sigma_2 & \\ & i\sigma_2 \end{pmatrix}, \quad (22)$$

where σ_2 is the second Pauli matrix. For any space-inversion-odd form factor, it follows immediately that $\Phi_a(\mathbf{k}) = 0$ at a high-symmetry point. Hence, the Hamiltonian at this high symmetry point is simply $\mathcal{H}_{eff}(\mathbf{k}_m^*) = (\xi_{\mathbf{k}_m^*} + \varepsilon_f)I/2 + (\xi_{\mathbf{k}_m^*} - \varepsilon_f)P/2$, where I is the four-dimensional identity matrix.

The parity at a high symmetry point is thus determined by $\delta_m = \text{sgn}(\xi_{\mathbf{k}_m^*} - \varepsilon_f)$. Four independent Z_2 topological indices ($\nu_0; \nu_1, \nu_2, \nu_3$)³⁹, one strong ($a = 0$) and three weak indices ($a = 1, 2, 3$) can be constructed from δ_m : (i) The strong topological index is the product of all eight

δ_m 's: $I_{\text{STI}} = (-1)^{\nu_0} = \prod_{m=1}^8 \delta_m = \pm 1$; (ii) by setting $k_j = 0$ (where $j = x, y, \text{ and } z$), three high-symmetry planes, $P_j = \{\mathbf{k} : k_j = 0\}$, are formed that contain four high-symmetry points each. The product of the parities at these four points defines the corresponding weak-topological index, $I_{\text{WTI}}^a = (-1)^{\nu_a} = \prod_{\mathbf{k}_m \in P_j} \delta_m = \pm 1$, $a = 1, 2, 3$ with integers corresponding to the axes x, y and z .

The existence of the three weak topological indices in 3D is related to a Z_2 topological index for 2D systems (a weak 3D TI is similar to a stack of 2D Z_2 topological insulators). Because there are three independent ways to stack 2D layers to form a 3D system, the number of independent weak topological indices is

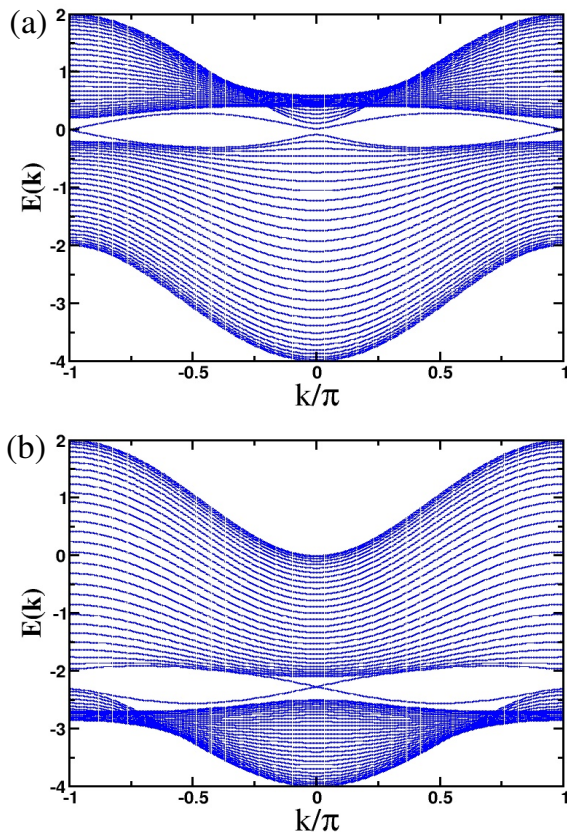


FIG. 2: Single particle band spectrum governed by the mean field Hamiltonian (21) along the x -axis, $k = k_x, k_y = 0$. Top panel shows the band structure for the weak topological insulator with the two Dirac points at the Brillouin zone boundaries. Band structure for the strong topological insulator with the Dirac point inside the band gap (bottom panel).

also three. A conventional band insulator has all of the four indices $I_{\text{STI}} = I_{\text{WTI}}^x = I_{\text{WTI}}^y = I_{\text{WTI}}^z = +1$ or equivalently $(0;0,0,0)$. An index $I = (-1)$ ($\nu_a = 1$) indicates a Z_2 topological state with the odd number of surface Dirac modes. In a KI the symmetry index δ_m of a particular high symmetry point m is negative provided $\xi_{\mathbf{k}_m^*} < \epsilon_f$ is lower the f -energy ϵ_f . Thus if $\xi_{\mathbf{k}_m^*=0} < \epsilon_f$ at the Γ point, while $\xi_{\mathbf{k}_m^*\neq 0} > \epsilon_f$ for all other symmetry points, then $I_{\text{STI}} = -1$, and hence the Kondo insulating state is a strong-topological insulator, robust against disorder Fig. 1. Weak-topological insulators and topologically trivial insulators can in principle be found for different band structures and different values of ϵ_f . A particularly interesting possibility is to tune topological phase transitions between different types of insulators (e.g., by applying a pressure). Although we have been specifically considering a tight-binding model with a primitive unit cell, all our conclusions apply directly to systems adiabatically connected to this model.

C. surface state calculation

In addition to the method discussed by us in Ref.²⁰, this can be proven by the direct calculation of the band spectrum together with the calculation of the entanglement entropy (see below). In what follows, we will assume that the f -electrons have very weak hole-like dispersion, i.e. $\epsilon_f \rightarrow \epsilon_{f\mathbf{k}} = 2t_f \sum_{i=x,y,z} \cos k_i + \mu_f$, where $t_f = 0.1t$ and μ_f is a chemical potential. This implies, in particular, the the boundary separating the WTI and STI are now given by $\mu'_c = \pm 2(t + t_f)$. Here, as before, the value of μ'_c is taken relative to the chemical potential of the conduction electrons.

In order to demonstrate that there is a metallic surface state in the spectrum described by the Hamiltonian (21) we consider a stack of $N = 30$ planes along the z -direction and diagonalize the Hamiltonian. The resulting Hamiltonian matrix has blocks along the diagonal, which describe the hopping and hybridization within each plane and the off-diagonal parts describing the hopping and hybridization between the planes. I For the set of the parameters corresponding to the strong topological Kondo insulator we compute the spectrum numerically and show the results on Fig. 2. For simplicity we have chosen the model form factor, given by:

$$\underline{\Phi} = \begin{cases} V(\sin k_x \sigma_x + \sin k_y \sigma_y), & \text{within the planes,} \\ iV_z \sigma_z, & \text{between the planes (upwards),} \\ -iV_z \sigma_z, & \text{between the planes (downwards).} \end{cases} \quad (23)$$

We see that for the case of strong topological insulator there appears a Dirac point in the gap in the middle of the Brillouin zone (BZ). For the set of parameters giving a weak topological insulators, there are two Dirac points located at the edges of the BZ. We note that the Dirac node in the spectrum exists not only for the simple cubic unit cell, but also for the more complicated fcc- and bcc-unit cells.

D. entanglement entropy and spectrum

In this Section we independently re-derive our results from the previous subsections by employing the concept of the entanglement entropy. In discussions on topological insulators without electron-electron interactions it is implicitly assumed that the presence of the gapless edge modes is a signature of the topologically non-trivial insulating state. In fact, this assumption is confirmed within our description of Kondo insulators. It is interesting, however, to check the topological properties of our model by discussing the properties of the eigenfunctions only. Such an approach has been pioneered by Freedman and collaborators⁴⁰ who showed that topologically nontrivial states of matter can exist without exhibiting the chiral edge modes. In this and the following Section we will discuss in detail the topological properties of the eigenfunctions governed by our effective model Hamiltonian (21).

As it has been extensively discussed in the literature (for the more recent accounts see [41–43] and references therein), entanglement entropy can be used to distinguish the topological phases from the non-topological ones. The following criterion

is used: the topologically nontrivial state should have non-zero entanglement entropy when the latter can not be tuned to zero by an adiabatic change of the parameters of the system⁴³.

As an aside, we note that our effective Hamiltonian (21) is a single-particle Hamiltonian and therefore, by calculating its entanglement spectrum we can also test the idea of adiabatic connectivity between our interaction-driven topological Kondo insulators and non-interacting topological insulators. The latter, however, cannot be adiabatically connected to trivial band insulators without making the system gapless. Note, for the trivial insulators we adopt the following definition⁴³: upon adiabatic change in the hopping elements to zero, a trivial insulator goes into an atomic insulator without closing the energy gap along the adiabatic path.

The entanglement entropy can be generally written as

$$S_{ent} = - \sum_a (\xi_a \log \xi_a + (1 - \xi_a) \log(1 - \xi_a)), \quad (24)$$

where $\{\xi_a\}$ are the single-particle entanglement eigenvalues, subscript a labels the eigenstates. When the entanglement eigenvalues are neither zero or one, the entanglement entropy is non-zero and therefore the system is topologically non-trivial. In particular, for translationally invariant topological insulator the spacial cut reveals the surface states and yields non zero entanglement entropy^{42,43}. In this case the entanglement eigenvalues are also labeled by the conserved components of the momentum, say, $\xi_a(k_x, k_y)$ for the cut in the xy -plane. Thus the problem of checking whether the insulator is topological or not reduces to the problem of determining the entanglement eigenvalues. For the case of the Kondo insulators, the computation of the entanglement spectrum may serve as an additional indicator of the nontrivial nature of their ground state especially for the case of complicated lattice structure when the simple approaches for the computation of the Z_2 indices do not apply. The procedure of how these eigenvalues are computed will be given below.

In this Section we will evaluate the entanglement entropy for the mean field Hamiltonians (21). using the Peschel's method⁴²⁻⁴⁴. The entanglement spectrum is determined by correlation function

$$G_{ij}^{\alpha\beta} = \langle \hat{\psi}_{i\alpha}^\dagger \hat{\psi}_{j\beta} \rangle, \quad (25)$$

where $\hat{\psi}_{i\alpha}$ creates an electron in state $\alpha = 1, \dots, 4$ (conduction or f - electron with spin up or down) on site i and the expectation value is evaluated in the ground state. Introducing the normal operators $\gamma_{n\mathbf{k}}$, where n is the number of the eigenvalues:

$$\hat{\psi}_{i\alpha} = \sum_{n=1}^{N_b} e^{i\mathbf{k}\cdot\mathbf{r}_i} u_{n\alpha}(\mathbf{k}) \hat{\gamma}_{n\mathbf{k}}, \quad (26)$$

where $N_b = 2$ is the number of the occupied bands and $u_{n\alpha}(\mathbf{k})$ are the eigenvectors. For the correlation function we find

$$G_{ij}^{\alpha\beta} = \sum_{\mathbf{k}} e^{i\mathbf{k}\cdot(\mathbf{r}_i - \mathbf{r}_j)} \sum_{n=1}^2 u_{n\alpha}^*(\mathbf{k}) u_{n\beta}(\mathbf{k}) \quad (27)$$

summation goes over all components of the momentum \mathbf{k} .

Let us imagine now that our system is cut in two halves along a given spacial directions. To be specific, let us make the cut along the xy -plane, so that k_x and k_y are conserved. The entanglement spectrum $\xi_a(\mathbf{k}_\perp)$, $\mathbf{k}_\perp = (k_x, k_y)$ Eq. (24), will then be given by the eigenvalues of the following matrix:

$$G_{ij}^{\alpha\beta}(k_x, k_y) = \sum_{k_z} e^{ik_z(z_i - z_j)} \sum_{n=1}^2 u_{n\alpha}^*(\mathbf{k}) u_{n\beta}(\mathbf{k}) \quad (28)$$

where i, j are confined to the right (or left) part of the system. Specifically, we need to solve the following eigenvalue problem:

$$\sum_{j,\beta} G_{ij}^{\alpha\beta}(\mathbf{k}_\perp) \varphi_{j\beta}^{(a)}(\mathbf{k}_\perp) = \xi_a(\mathbf{k}_\perp) \varphi_{i\alpha}^{(a)}(\mathbf{k}_\perp) \quad (29)$$

We show the results of our computation for the model Hamiltonian (21) with $N_b = 2$ on Figs. 3 and 4. As we can see, depending on the position of renormalized f -level relative to the bottom of the conduction band, we find either single node or two nodes in the entanglement spectrum. The number of the nodes is equal to the number of nodes of the surface states inside the insulating gap, in complete agreement with our expectations.

To summarize, our results from this Section confirm that Z_2 -odd topological Kondo insulators cannot be adiabatically connected to Z_2 -even insulators adiabatically without vanishing of the insulating gap along the adiabatic path. At the same time we see one-to-one correspondence between the Kondo insulators and non-interacting Z_2 topological insulators confirming the idea of adiabatic connectivity between the two discussed in the Introduction.

IV. CONSTRUCTION OF THE WANNIER WAVE FUNCTIONS

Within our model of Kondo insulators we can also address the problem of constructing maximally localized Wannier functions (WF). This question has several important applications in the general theory of topological insulators^{45,46}, such as calculation of the Z_2 indices as well as characterization of the topological structure using first principles calculations.

Generally, the construction of the WF proceeds in two stages. The first stage has to do with the initial choice of the basis set before specifying a particular choice of the gauge. This needs to be done in order to make the WF nonsingular across the whole Brillouin zone. The gauge is then fixed by imposing the certain criterion. As an example, maximum localization criterion is typically used⁴⁷. Apart from the problem related to the arbitrariness in the choice of Wannier functions, there exists a topological obstruction for constructing the Wannier functions for Chern insulators realized in systems with broken time-reversal symmetry^{48,49}. As it turns out, in the case of the Z_2 topological insulators there is also a topological obstruction albeit a less severe one. As it was recently

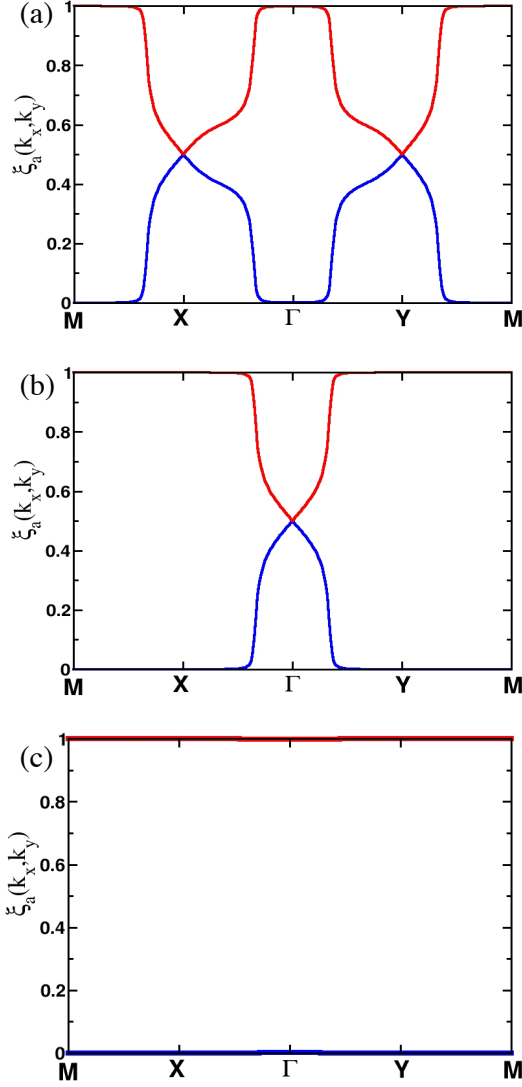


FIG. 3: Entanglement spectrum for the model of Ce-based Kondo insulator: (a) weak topological insulator (0; 111), (b) strong topological insulator (1; 000) and (c) trivial insulator (0; 000). For the presentation purposes we choose only two eigenvalues for each momentum \mathbf{k}_\perp .

discussed in Ref. [45] for the Kane-Mele model, it is impossible to construct the time-reversal invariant basis set of the Wannier functions, but one can construct the basis set consisting of the non-Kramers pairs. The above mentioned arbitrariness in the definition of the WF is then fixed by the criterion of maximum localization^{46,47}.

In this section we will specifically apply the prescription developed in Ref. [45] to construct the basis set which then can be used to initialize the procedure to compute the maximum localized WF. On one hand, this should provide another example of the manifestation of above mentioned obstruction and the way it can be resolved. On the other hand, it gives an insight into the structure of the wave functions describing the quasiparticles in the occupied bands.

A. preliminaries

Below we will follow almost verbatim the discussion in Refs. [45,47]. For variety of applications (i.e. numerical calculations) it is required that the Bloch-like wave functions must remain smooth across the whole Brillouin zone (BZ). The problem is that the specific choice of the Bloch functions $|\psi_{n\mathbf{k}}\rangle$ is not unique, since these wave functions have an additional gauge freedom originating from possibility of mixing with the wave functions describing the occupied bands:

$$|\psi_{n\mathbf{k}}\rangle \rightarrow \sum_m U_{nm}(\mathbf{k}) |\psi_{m\mathbf{k}}\rangle \quad (30)$$

(here the summation goes over the occupied bands). For all the practical purposes, however, the freedom of choosing the proper gauge transformation must be removed by applying some restrictions on choosing the specific gauge. The latter uses the criterion of maximum localization of the WF⁴⁷. WFs are defined by

$$W_n(\mathbf{r} - \mathbf{R}) = \frac{\Omega}{(2\pi)^3} \int_{BZ} e^{-i\mathbf{k}\cdot\mathbf{R}} \psi_{n\mathbf{k}}(\mathbf{r}), \quad (31)$$

where Ω is a volume of the unit cell and $\psi_{n\mathbf{k}}(\mathbf{r}) = \langle \mathbf{r} | \psi_{n\mathbf{k}} \rangle$ are the Bloch wave functions, n is a band index and \mathbf{R} is a position of a lattice site.

The unitary transformation (30) can be initialized using the following procedure. One first chooses the set of localized trial wave functions $|\tau_{i\mathbf{k}}\rangle$ and then form a set of new basis functions

$$|\tilde{\tau}_{i\mathbf{k}}\rangle = \sum_{n=1}^{\mathcal{N}} |\psi_{n\mathbf{k}}\rangle \langle \psi_{n\mathbf{k}} | \tau_{i\mathbf{k}} \rangle, \quad i = 1, \mathcal{N} \quad (32)$$

where \mathcal{N} is the number of the occupied bands. Since this new basis set is not orthonormal, one can adopt a Löwdin procedure and form the overlap matrix

$$S_{mn}(\mathbf{k}) = \langle \tilde{\tau}_{m\mathbf{k}} | \tilde{\tau}_{n\mathbf{k}} \rangle. \quad (33)$$

Now we can use Eqs. (32,33) to form a set of Bloch-like states

$$|\tilde{\psi}_{n\mathbf{k}}\rangle = \sum_m \left[S^{-1/2}(\mathbf{k}) \right]_{mn} |\tilde{\tau}_{m\mathbf{k}}\rangle \quad (34)$$

These states, albeit not eigenstates of the Hamiltonian, should be the smooth functions of the quasi-momentum \mathbf{k} and are used to construct the localized set of the WFs:

$$\tilde{W}_n(\mathbf{r} - \mathbf{R}) = \frac{\Omega}{(2\pi)^3} \int_{BZ} e^{-i\mathbf{k}\cdot\mathbf{R}} \tilde{\psi}_{n\mathbf{k}}(\mathbf{r}) \quad (35)$$

The above construction breaks if the determinant of the matrix $S_{mn}(\mathbf{k})$ vanishes in some points of the BZ. Thus the problems consists in finding the proper set of trial states (32) such that $\det[S(\mathbf{k})] \neq 0$. Finally, we note that required degree of localization can be achieved by employing the iterative procedure⁴⁷.

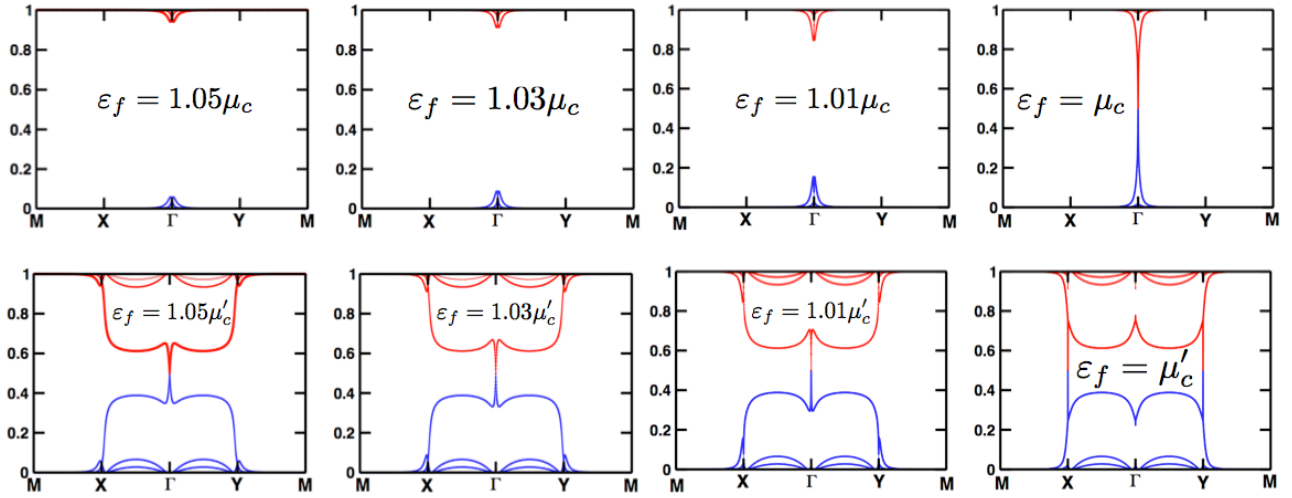


FIG. 4: Evolution of the entanglement spectrum with the change in the position of the renormalized f -level, ε_f . Top four panels show the change in the entanglement spectrum as the system goes from the trivial insulator to the strong topological insulator. Bottom four panels illustrate the changes in spectrum as system goes from strong to weak topological insulator. Note that when ε_f is exactly at the boundary separating different insulating phases so that the bulk insulating gap vanishes, the vertical lines in the entanglement entropy spectrum reflect the absence of the surface modes at the boundaries.

We now construct the Wannier functions for our mean field model described by the Hamiltonian (21). For the Bloch wave functions we write

$$|\psi_{n\mathbf{k}}\rangle = \sum_{s=1}^4 C_{s n \mathbf{k}} |s\mathbf{k}\rangle, \quad (36)$$

where $n = 1, 2$ labels the occupied bands, coefficients $C_{s n \mathbf{k}}$ are the components of the eigenvectors of the Hamiltonian (21) and the summation goes over the components of generalized spinor which includes spinfull conduction (c) and f -electron (f) states:

$$\begin{aligned} |s = 1, \mathbf{k}\rangle &= \hat{c}_{\mathbf{k}\uparrow}^\dagger |0\rangle, & |s = 2, \mathbf{k}\rangle &= \hat{c}_{\mathbf{k}\downarrow}^\dagger |0\rangle, \\ |s = 3, \mathbf{k}\rangle &= \hat{f}_{\mathbf{k}\uparrow}^\dagger |0\rangle, & |s = 4, \mathbf{k}\rangle &= \hat{f}_{\mathbf{k}\downarrow}^\dagger |0\rangle \end{aligned} \quad (37)$$

In Eq. (36) the basis functions $|s\mathbf{k}\rangle$ are defined on the each site on the lattice \mathbf{R} , i.e.

$$|s\mathbf{k}\rangle = \frac{|s\rangle}{\sqrt{N}} \sum_{\mathbf{r}} e^{i\mathbf{k}\cdot\mathbf{r}} \delta(\mathbf{r} - \mathbf{R}) \quad (38)$$

In what follows we adopt the method outlined above to construct the Wannier functions for our model Kondo insulators.

B. choice of the basis

Onset of the coherence in the Kondo lattice can be interpreted as an emergence of new quasi-particles which are the linear superposition of the localized and conduction states. Since the newly formed quasiparticle band is narrow, the spectral weight is mostly governed by the f -states. Thus, to construct the Wannier functions we first consider the basis on f -states only:

$$|\tau_{1\mathbf{k}}\rangle = |3\mathbf{k}\rangle, \quad |\tau_{2\mathbf{k}}\rangle = |4\mathbf{k}\rangle \quad (39)$$

(see Eqs. (37,38)). For the new set of basis vectors (32) with the help of Eqs. (36,39) this implies

$$\begin{aligned} |\tilde{\tau}_{1\mathbf{k}}\rangle &= C_{31\mathbf{k}}^* |\psi_{1\mathbf{k}}\rangle + C_{32\mathbf{k}}^* |\psi_{2\mathbf{k}}\rangle, \\ |\tilde{\tau}_{2\mathbf{k}}\rangle &= C_{41\mathbf{k}}^* |\psi_{1\mathbf{k}}\rangle + C_{42\mathbf{k}}^* |\psi_{2\mathbf{k}}\rangle, \end{aligned} \quad (40)$$

For the determinant of the matrix $\hat{S}(\mathbf{k})$ we find

$$\begin{aligned} \det[\hat{S}(\mathbf{k})] &= (|C_{31\mathbf{k}}|^2 + |C_{32\mathbf{k}}|^2)(|C_{41\mathbf{k}}|^2 + |C_{42\mathbf{k}}|^2) \\ &\quad - |C_{31\mathbf{k}}C_{41\mathbf{k}}^* + C_{32\mathbf{k}}C_{42\mathbf{k}}^*|^2 \end{aligned} \quad (41)$$

We present the results on Fig. 5. We see that the determinant of the matrix (33) is zero near the Γ -point which means that the choice (39) is not suitable for construction of non-singular Bloch functions and consequently Wannier functions. The same result holds for the trial basis built out of the conduction states, $|1\mathbf{k}\rangle$ and $|2\mathbf{k}\rangle$ as well as their linear combinations.

As we have mentioned above, formation of the coherence in the Kondo lattice can be seen as a formation of the new states (or quasiparticles) as a result of the hybridization between the conduction and f electrons. Motivated by this observation, let us try the following two trial basis wave-functions:

$$\begin{aligned} |\tau_{1\mathbf{k}}\rangle &= \frac{1}{\sqrt{2}}(|1\mathbf{k}\rangle + |3\mathbf{k}\rangle), \\ |\tau_{2\mathbf{k}}\rangle &= \frac{1}{\sqrt{2}}(|2\mathbf{k}\rangle - |4\mathbf{k}\rangle), \end{aligned} \quad (42)$$

Note that the trial basis functions do not transform into each other by time reversal operator, so they do not form a Kramers

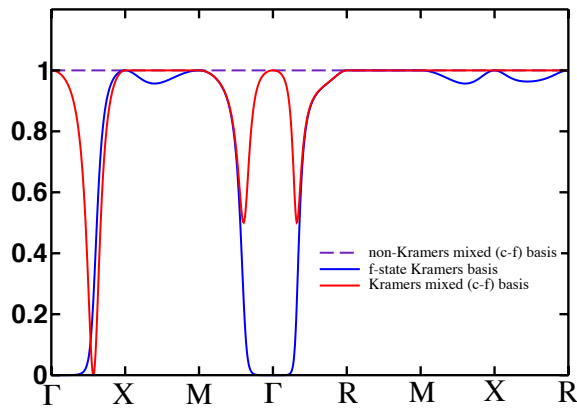


FIG. 5: Plot of the dependence of $\det[\hat{S}(\mathbf{k})]$ along the path in the BZ. The elements of the matrix $\hat{S}(\mathbf{k})$ has been obtained using the trial basis set, which consists of (a) non-Kramers pair of states each containing the superposition between the conduction and f -states; (b) Kramers pair of f -states and (c) Kramers pair states with linear superposition of conduction and f -electron wave functions. Determinant does not vanish anywhere in the BZ only for the basis (c).

doublet. It follows

$$\begin{aligned} |\tilde{\gamma}_{1\mathbf{k}}\rangle &= \frac{(C_{11\mathbf{k}}^* + C_{31\mathbf{k}}^*)}{\sqrt{2}} |\psi_{1\mathbf{k}}\rangle + \frac{(C_{12\mathbf{k}}^* + C_{32\mathbf{k}}^*)}{\sqrt{2}} |\psi_{2\mathbf{k}}\rangle, \\ |\tilde{\gamma}_{2\mathbf{k}}\rangle &= \frac{(C_{21\mathbf{k}}^* - C_{41\mathbf{k}}^*)}{\sqrt{2}} |\psi_{1\mathbf{k}}\rangle + \frac{(C_{22\mathbf{k}}^* - C_{42\mathbf{k}}^*)}{\sqrt{2}} |\psi_{2\mathbf{k}}\rangle, \end{aligned} \quad (43)$$

The determinant of the matrix $\hat{S}(\mathbf{k})$ up to the numerical prefactor is

$$\begin{aligned} \det[\hat{S}(\mathbf{k})] &= (|C_{11\mathbf{k}} + C_{31\mathbf{k}}|^2 + |C_{12\mathbf{k}} + C_{32\mathbf{k}}|^2) \times \\ & \quad (|C_{21\mathbf{k}} - C_{41\mathbf{k}}|^2 + |C_{22\mathbf{k}} - C_{42\mathbf{k}}|^2) - \\ & \quad - |(C_{11\mathbf{k}}^* + C_{31\mathbf{k}}^*)(C_{21\mathbf{k}} - C_{41\mathbf{k}}) + \\ & \quad + (C_{12\mathbf{k}}^* + C_{32\mathbf{k}}^*)(C_{22\mathbf{k}} - C_{42\mathbf{k}})|^2 \end{aligned} \quad (44)$$

We present the resulting dependence $\det[\hat{S}(\mathbf{k})]$ on momentum on Fig. 5. As we have expected, the determinant does not vanish anywhere within the BZ which means we have succeeded in constructing the wave functions $|\tilde{\psi}_{n\mathbf{k}}\rangle$ (34). In fact, we find $\det[\hat{S}(\mathbf{k})] = 1$ for the non-Kramers basis set (43). Finally, we note that in agreement to the results of Ref. [45] obtained for the Z_2 -odd phase in the Kane-Mele model, here our non-singular basis set also consists of the non-Kramers pair of states. To summarize, we have demonstrated that the basis for the Bloch wave functions can be chosen in such a way that no singularities are generated across the Brillouin zone.

V. CONCLUSIONS

In this paper we have discussed the conditions for the emergence of chiral surface states in semiconducting f -electron systems. We considered an insulating state in heavy fermion systems which appears at finite temperatures as a result of strong interaction between the conduction and the predominantly localized f -electrons. Having started with the periodic Anderson lattice model, we considered the low-energy version of that model, which takes into account the effect of Hubbard repulsion between the f -electrons on the level of renormalizations to the f -electron energy and hybridization amplitudes. The key ingredient of our model is momentum dependent hybridization amplitudes. The momentum dependence of the amplitudes originates from the strong spin-orbit coupling interaction on f -sites. The analysis of the topological structure of the newly formed insulating state is greatly simplified for the systems with simple cubic unit cell. In that case, the form factors vanish at high symmetry points of the BZ. This embeds the topological singularities into the valence band, so that when the form-factors have p - or f -wave symmetry it immediately leads to the topological insulator.

To describe the physics of Ce-based Kondo insulators, we considered the simplest model containing single conduction band hybridized with the Kramers doublet of f -states. We find that there will always be chiral surface states, when hybridization gap does not have nodes. The robustness of these states with respect to disorder is determined by the position of the renormalized f -level relative to the bottom of the conduction band. We then verify our results for both models by calculating the entanglement entropy spectrum. Finally, we also discuss how to choose the basis for constructing Wannier wave functions, which are well defined everywhere in the Brillouin zone. It is interesting to note that the required basis relies on superposition between the conduction and the localized f -states. More importantly, this agrees with common view that a heavy quasiparticle is the quantum many-body superposition of conduction and f -states.

VI. ACKNOWLEDGMENTS

We would like to thank D. Vanderbilt, J. Allen and M. Aronson for stimulating discussions. This work was supported by the Ohio Board of Regents Research Incentive Program grant OBR-RIP-220573 (M.D.), JQI-NSF-PFC (K. S.), DOE grant DE-FG02-99ER45790 (P. C.), and NSF-CAREER (V.G.). This work was supported in part by the National Science Foundation under grant No. 1066293 and the hospitality of the Aspen Center for Physics.

¹ M. Z. Hasan and C.L. Kane, Rev. Mod. Phys. **82**, 3045 (2010).

² X.-L. Qi and S.-C. Zhang, Rev. Mod. Phys. **83**, 1057 (2011).

³ L. Fu, C. L. Kane and E. J. Mele, Phys. Rev. Lett. **98**, 106803 (2007).

- ⁴ J. E. Moore and L. Balents, Phys. Rev. B **75**, 121306(R) (2007).
- ⁵ R. Roy, Phys. Rev. B **79**, 195322 (2009).
- ⁶ D. Hsieh, D. Qian, L. Wray, Y. Xia, Y. S. Hor, R. J. Cava and M. Z. Hasan, Nature **452**, 970 (2008).
- ⁷ Y. Xia, D. Qian, D. Hsieh, L. Wray, A. Pal, H. Lin, A. Bansil, D. Grauer, Y. S. Hor, R. J. Cava and M. Z. Hasan, Nat. Phys. **5**, 398 (2009).
- ⁸ P. Roushan, J. Seo, C. V. Parker, Y. S. Hor, D. Hsieh, D. Qian, A. Richardella, M. Z. Hasan, R. J. Cava and A. Yazdani, Nature **460**, 1106 (2009).
- ⁹ T. Zhang, P. Cheng, X. Chen, J. F. Jia, X. C. Ma, K. He, L. L. Wang, H. J. Zhang, X. Dai, Z. Fang, X. C. Xie and Q. K. Xue, Phys. Rev. Lett. **103**, 266803 (2009).
- ¹⁰ J. Seo, P. Roushan, H. Beidenkopf, Y. S. Hor, R. J. Cava, and A. Yazdani, Nature **466**, 343 (2010).
- ¹¹ Z. Alpichshev, J. G. Analytis, J. H. Chu, I. R. Fisher, Y. L. Chen, Z. X. Shen, A. Fang and A. Kapitulnik, Phys. Rev. Lett. **104**, 016401 (2010).
- ¹² S. Raghu, X.-L. Qi, C. Honerkamp, S.-C. Zhang, Phys. Rev. Lett. **100**, 156401 (2008).
- ¹³ K. Sun, H. Yao, E. Fradkin and S. A. Kivelson, Phys. Rev. Lett. **103**, 046811 (2009).
- ¹⁴ R. Nandkishore and L. Levitov Phys. Rev. B **82**, 115124 (2010).
- ¹⁵ K. Sun, W. Vincent Liu and S. Das Sarma, e-print arXiv:1011.4301.
- ¹⁶ H. M. Guo and M. Franz, Phys. Rev. Lett. **103**, 206805 (2009).
- ¹⁷ D. A. Pesin and L. Balents, Nat. Phys. **6**, 376 (2010).
- ¹⁸ X. A. Wan, A. Turner, A. Vishwanath and S. Y. Savrasov, e-print arXiv: 1007.0016.
- ¹⁹ B.-J. Yang and Y. B. Kim, e-print arXiv:1004.4630.
- ²⁰ M. Dzero, K. Sun, V. Galitski and P. Coleman, Phys. Rev. Lett. **104**, 106408 (2010).
- ²¹ Binghai Yan, Lukas Muechler, Xiao-Liang Qi, Shou-Cheng Zhang and Claudia Felser, e-print arXiv:1104:0641.
- ²² J. N. Chazalviel, M. Campagna, G. K. Wertheim, and P. H. Schmidt, Phys. Rev. B **14**, 4586 (1976).
- ²³ A. Menth, E. Buehler and T. H. Geballe, Phys. Rev. Lett. **22**, 295 (1969).
- ²⁴ G. Aeppli and Z. Fisk, Comm. Condens. Matter Phys. **16**, 155 (1992).
- ²⁵ H. Tsunetsugu, M. Sigrist and K. Ueda, Rev. Mod. Phys. **69**, 809 (1997).
- ²⁶ P. Riseborough, Adv. Phys. **49**, 257 (2000).
- ²⁷ P. Coleman, "Heavy Fermions: Electrons at the Edge of Magnetism", Handbook of Magnetism and Advanced Magnetic Materials, Vol 1, 95-148 (Wiley, 2007).
- ²⁸ R. Martin and J. Allen, J. Appl. Phys. **50**, 7561 (1979).
- ²⁹ X. Wan, A. M. Turner, A. Vishwanath and S. Y. Savrasov, Phys. Rev. B **83**, 205101 (2011).
- ³⁰ K. A. Kikoin, A. de Visser, K. Bakker, T. Takabatake, Z. Phys. B **94**, 79 (1994).
- ³¹ H. Ikeda and K. Miyake, Jour. of Phys. Soc. of Japan **65**, 1769 (1996).
- ³² Juana Moreno and P. Coleman, Phys. Rev. Lett. **84**, 342 (2000).
- ³³ E. D. Bauer, A. D. Christianson, J. M. Lawrence, E. A. Goremychkin, N. O. Moreno, N. J. Curro, F. R. Trouw, J. L. Sarrao, J. D. Thompson, R. J. McQueeney, W. Bao and R. Osborn, J. Appl. Phys. bf 95, 7201 (2004).
- ³⁴ B. Coqblin and J. R. Schrieffer, Phys. Rev. **185**, 847 (1969).
- ³⁵ Rebecca Flint, M. Dzero, and P. Coleman, Nature Physics **4**, 643 (2008).
- ³⁶ M. F. Hundley, P. C. Canfield, J. D. Thompson, and Z. Fisk Phys. Rev. B **42**, 6842 (1990).
- ³⁷ T. Terashima, C. Terakura, S. Uji, H. Aoki, Y. Echizen and T. Takabatake, Phys. Rev. B **66**, 075127 (2002).
- ³⁸ L. Fu and C. L. Kane, Phys. Rev. B **76**, 045302 (2007).
- ³⁹ A. Kitaev, e-print arXiv:0901.2686v2 (2009).
- ⁴⁰ M. Freedman, C. Nayak, K. Shtengel and K. Walker, Ann. Phys. **310**, 428 (2004).
- ⁴¹ H. Li and F. D. M. Haldane, Phys. Rev. Lett. **101**, 010504 (2008).
- ⁴² Ari M. Turner, Yi Zhang and Ashvin Vishwanath, e-print arXiv:0909:3119.
- ⁴³ T. Hughes, E. Prodan and B. A. Bernevig, e-print arXiv:1010.4508.
- ⁴⁴ I. Peschel, J. Stat. Mech. **10**, P06004 (2004).
- ⁴⁵ A. Soluyanov and D. Vanderbilt, e-print arXiv:1009:1415.
- ⁴⁶ R. Yu, X. L. Qi, A. Bernevig, Z. Feng and X. Dai, preprint arXiv:1101.2011 (2011).
- ⁴⁷ N. Marzari and D. Vanderbilt, Phys. Rev. B **56**, 12847 (1997).
- ⁴⁸ T. Thonhauser and D. Vanderbilt, Phys. Rev. B **74**, 235111 (2006).
- ⁴⁹ J. D. Thouless, J. Phys. C **17**, 235 (1984).